The Hunga Tonga-Hunga Ha'apai Hydration of the Stratosphere

L. Millán[1], M. L. Santee[1], A. Lambert[1], N. J. Livesey[1], F. Werner[1], M. J. Schwartz[1], H. C. Pumphrey[2], G. L. Manney[3,4], Y. Wang[5,1], H. Su[1], L. Wu[1], W. G. Read[1], and L. Froidevaux[1]

[1]Jet Propulsion Laboratory, California Institute of Technology, Pasadena, California, USA
[2]School of GeoSciences, The University of Edinburgh, Edinburgh, UK
[3]NorthWest Research Associates, Socorro, New Mexico, USA
[4]New Mexico Institute of Mining and Technology, Socorro, New Mexico, USA
[5]Division of Geological and Planetary Sciences, California Institute of Technology, Pasadena, CA, USA

Key Points:

- Following the Hunga Tonga-Hunga Ha'apai eruption, the Aura Microwave Limb Sounder measured enhancements of stratospheric H_2O, SO_2, and HCl
- The mass of SO_2 and HCl injected is comparable to that from prior eruptions, whereas the magnitude of the H_2O injection is unprecedented
- Excess stratospheric H_2O will persist for years, could affect stratospheric chemistry and dynamics, and may lead to surface warming

Corresponding author: L. Millán, `lmillan@jpl.nasa.gov`

Abstract

Following the 15 January 2022 Hunga Tonga-Hunga Ha'apai eruption, several trace gases measured by the Aura Microwave Limb Sounder displayed anomalous stratospheric values. Trajectories and radiance simulations confirm that the H_2O, SO_2, and HCl enhancements were injected by the eruption. In comparison with those from previous eruptions, the SO_2 and HCl injections were unexceptional, although they reached higher altitudes. In contrast, the H_2O injection was unprecedented in both magnitude (far exceeding any previous values in the 17-year MLS record) and altitude (penetrating into the mesosphere). We estimate the mass of H_2O injected into the stratosphere to be $146\pm5\,\mathrm{Tg}$ — $\sim$10% of the stratospheric burden. It may take several years for the H_2O plume to dissipate. This eruption could impact climate not through surface cooling due to sulfate aerosols, but rather through surface warming due to the radiative forcing from the excess stratospheric H_2O.

Plain Language Summary

The violent Hunga Tonga-Hunga Ha'apai eruption on 15 January 2022 injected not only ash into the stratosphere but also large amounts of water vapor, breaking all records for direct injection of water vapor, by a volcano or otherwise, in the satellite era. This is not surprising since the Hunga Tonga-Hunga Ha'apai caldera was formerly situated 150 meters below sea level. The massive blast injected water vapor up to altitudes as high as $53\,\mathrm{km}$. Using measurements from the Microwave Limb Sounder on NASA's Aura satellite, we estimate that the excess water vapor is equivalent to around 10% of the amount of water vapor typically residing in the stratosphere. Unlike previous strong eruptions, this event may not cool the surface, but rather it could potentially warm the surface due to the excess water vapor.

1 Introduction

Hunga Tonga-Hunga Ha'apai (HT-HH), a submarine volcano in the South Pacific (20.54°S, 175.38°W), reached its climactic eruption phase on 15 January 2022. The blast sent a volcanic plume into the mesosphere to altitudes of up to $57\,\mathrm{km}$ — a record in the satellite era (Carr et al., 2022; Proud et al., 2022). It also triggered tsunami alerts across the world (Ramirez-Herrera et al., 2022; Carvajal et al., 2022), waves that propagated globally (Wright et al., 2022), and ionospheric disturbances (Themens et al., 2022). Details about the HT-HH caldera complex, seismology, and volcanology are given by Kusky (2022) and Yuen et al. (2022).

In addition to particulate matter, volcanic eruptions can loft large quantities of gases into the stratosphere. Although around 80% of this gas volume can be magmatic H_2O (Pinto et al., 1989; Coffey, 1996), up to 90% of the volcanically emitted humidity is usually removed by condensation at the cold point tropopause (Glaze et al., 1997). Considerable amounts of CO_2 and SO_2 are also often found in volcanic plumes, along with HCl and other trace gases (e.g., Carn et al., 2016). SO_2 reacts with H_2O and OH to form submicron sulfate aerosols that reflect solar radiation, lowering surface temperature. For example, the radiative influence of the 1991 Mount Pinatubo eruption "put an end to several years of globally warm surface temperature" (McCormick et al., 1995), illustrating the capacity of volcanic eruptions to substantially alter global climate.

The composition of the HT-HH plume is unprecedented, as the eruption injected vast amounts of H_2O directly into the stratosphere. The high moisture content of the plume is perhaps not surprising, since the HT-HH caldera was situated $150\,\mathrm{m}$ below sea level (Cronin et al., 2017), where water in contact with the erupting magma (at temperatures of $\sim$1100–1470 K) was superheated, resulting in explosive steam.

The Microwave Limb Sounder (MLS) onboard NASA's Aura satellite provides measurements of 15 trace gases, among them H_2O, HCl, and enhanced volcanic SO_2. MLS measures thermal emission from the Earth's limb, covering spectral regions near 118, 190, 240, and 640 GHz (Waters et al., 2006). MLS is well suited to observe volcanic plumes, since microwave radiances are largely unaffected by sulfate aerosols. Moreover, the MLS two-dimensional retrieval exploits overlapping limb observations to better constrain trace gas gradients (Livesey et al., 2006), allowing the spatial heterogeneity of the plume to be captured.

Here, we use MLS version 4 (v4) data, instead of the most recent version 5 (v5). In the v4 190-GHz retrievals, tangent point pressure information is taken from earlier retrievals considering O_2 spectral lines, while v5 retrievals update this information in light of measurements of H_2O emission. Poor fits to these signals in regions with extremely enhanced H_2O, such as those discussed here, lead to discrepancies in tangent pointing information as large as ~2.5 km, degrading the accuracy of the H_2O, N_2O, HNO_3, and HCN retrievals in v5.

2 Validity of MLS Measurements After the Eruption

Ten hours after the eruption on 15 January, MLS measured enhanced values of H_2O at altitudes up to 0.46 hPa (~53 km), well above the stratopause (Figure 1c). Most of these measurements of enhanced H_2O did not pass the MLS quality screening (QS) criteria defined by Livesey et al. (2020), indicating that the retrieval achieved only a poor fit to the radiances. The poor performance of the standard data processing algorithms is unsurprising, as the largest H_2O values are more than an order of magnitude greater than any previously observed by MLS and more than 100 standard deviations above background levels. Here data points with values greater than 7 standard deviations above the climatological January-February-March (JFM) 2005–2021 average are identified as enhancements.

The eruption injected H_2O throughout a large vertical range encompassing most of the stratosphere, but on 15 January MLS only measured the outer edge of the plume in the upper stratosphere, where strong winds advected the lofted H_2O to locations sampled by MLS. Near 80 hPa on this day, MLS also measured some enhanced H_2O injected by a previous, less violent, HT-HH eruption on 14 January.

For the next several days, most of the largest enhancements failed the QS. Figure 1d shows the profiles displaying the largest mixing ratios on 15, 16, 17, and 18 January. Back trajectories (as in Livesey et al. (2015); Santee et al. (2022)) indicate that these enhancements lie downwind from the HT-HH volcano (Figure 1b), and the measured spectral signature is well represented by radiance simulations (Figure 1e). Peaks centered on channels 5 and 22 on 16 and 17 January are SO_2 spectral lines; they indicate that these lower plumes contained more SO_2 than the high-altitude plume on 15 January.

As the plume dispersed, the daily number of profiles failing the QS increased, reaching a maximum on 19 January. Retrieval performance then returned to normal by 8 February, by which time the plume had dispersed sufficiently that maximum H_2O values had dropped to ~50 ppmv, versus up to 350 ppmv immediately following the eruption (Figure 1).

Taken together, the back trajectories, radiance simulations, and return to typical retrieval quality confirm that the measured enhancements represent real volcanically enhanced H_2O values. However, the absolute magnitudes of the enhancements, especially for those failing the QS screening, are still in question because of the poor radiance fits. The MLS retrievals were not optimized to handle such strong H_2O enhancements. Thus, to fully quantify these injections and their uncertainties, we are developing a special re-
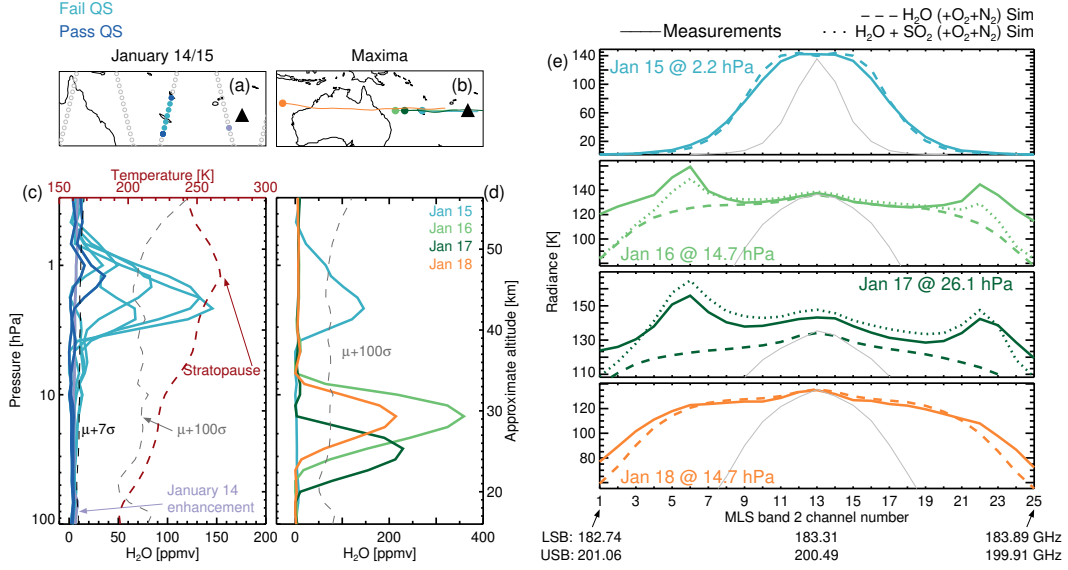
Figure 1. (a) Location of observed H_2O enhancements on 14 and 15 January. (b) Location of maximum H_2O on 15, 16, 17, and 18 January. Lines display back trajectories from these measurements to the eruption time. (c) H_2O profiles associated with locations shown in (a). The temperature profile (red dashed line) is the average of the temperature profiles retrieved by MLS at those locations. (d) H_2O profiles associated with locations shown in (b). The 2005–2021 JFM mean plus 100 standard deviation values ($\mu + 100\sigma$) are also shown in (c) and (d). (e) Measured (solid lines) and simulated (with and without considering SO_2, dotted and dashed lines, respectively) radiances at the mixing ratio maxima for the enhanced profiles shown in (d) (colored lines), as well as for background conditions at the same pressure levels (gray lines). Note that this MLS spectrometer is centered on the 183.3 GHz H_2O spectral line. Most MLS spectrometers observe emissions from two separate spectral regions: the "lower sideband" (LSB) and "upper sideband" (USB), as indicated for selected channels.

trieval for MLS measurements of the HT-HH plume. Preliminary results suggest that H_2O retrievals that better fit the radiances lie within 20% of current v4 estimates.

In addition, it is essential to account for the relatively coarse resolution of the MLS observations ($\sim 3.2 \times 230$ km for H_2O at these altitudes, as quantified by the averaging kernels (Livesey et al., 2020)) in the presence of strong vertically confined plumes (Schwartz et al., 2013, 2020). Accordingly, mid-January maximum plume values of 1500 ppmv measured by radiosondes (Sellitto et al., 2022) are not necessarily inconsistent with observed MLS abundances given the disparity in their respective resolutions.

Many chemical species measured by MLS show anomalous mixing ratios in the plume (Figure S1). However, only the H_2O, SO_2, and HCl spectral signatures can confidently be ascribed to real enhancements in those quantities; perturbations in other species are likely artifacts arising from SO_2 spectral interference. SO_2 is retrieved from a spectrometer that targets an $O^{18}O$ line but also covers many SO_2 lines, the strongest of which are located in channels 5, 11, and 20. The triple-peak structure in measured radiances within the volcanic plume (Figure 2b) can only be plausibly explained by an SO_2 enhancement.

HCl is currently measured by a spectrometer that targets an O_3 line but covers HCl lines in channels 3 and 25. The $\sim$5 K HCl radiance signature overlaps with an $\sim$180 K O_3 signal. The differences between the measurements and the simulations with and without accounting for contributions from HCl suggest that the observed enhancements represent real atmospheric signals (Figure 2d). The HCl spectral signature is similar to that of the background because the HCl enhancements are not as dramatic as those of H_2O or SO_2.

MLS estimates of ice water content (IWC) are based on the differences between the measured radiances and the expected clear-sky radiances, with the residuals attributed to ice scattering and/or ice absorption. The clear-sky radiances are calculated using the retrieved atmospheric states; since most retrievals in the volcanic plume fail the QS in the days following the eruption, the derived IWC estimates are unreliable. In contrast, the quality of the MLS temperature, CO, and O_3 measurements is not affected by the plume.

3 Unprecedented stratospheric H_2O injection

Figure 3 compares the HT-HH HCl, SO_2, and H_2O stratospheric injections to other stratospheric injections (volcanic or otherwise) observed by MLS. Large injections are marked individually.

The HT-HH eruption did not inject vast amounts of either HCl or SO_2 into the stratosphere. The total injected mass of stratospheric SO_2 (calculated as described by Pumphrey et al. (2021)) was 0.41±0.02 Tg, which pales in comparison to that from previous eruptions measured by MLS, such as the 2008 Kasatochi, the 2009 Sarychev, or the 2019 Raikoke eruptions, which each emitted $\sim$1 Tg (Pumphrey et al., 2015; de Leeuw et al., 2021). The mass of SO_2 injected by HT-HH is even less noteworthy in the context of the 17 Tg injected by the 1991 Pinatubo eruption (Read et al., 1993).

The only unusual aspect of the SO_2 plume is its injection height. SO_2 plumes are typically injected at altitudes no higher than 46 hPa ($\sim$21 km) (Carn et al., 2016; Pumphrey et al., 2015). HT-HH is the only injection observed by MLS that produced maximum values of SO_2 at 14 hPa ($\sim$29 km), with enhanced values detected up to 6.8 hPa ($\sim$35 km) — outside the normally recommended pressure range for MLS SO_2. By 27 January, the SO_2 plume dropped below background levels (Figure S1).

The HCl injection was similarly unremarkable, with only 8 profiles during 16–18 January (barely) exceeding the threshold for enhancement (Figure 2c; Figure S1). As with SO_2, the only unusual aspect of the HCl plume is its injection height of 31.6 hPa ($\sim$24 km), whereas previous eruptions reached no higher than 68 hPa ($\sim$18.6 km).

In contrast, the magnitude of the HT-HH H_2O injection is unprecedented. Three natural pathways for direct injection of H_2O into the stratosphere exist: overshooting convection, pyrocumulonimbus (pyroCb) storms, and volcanic eruptions. The previous stratospheric H_2O record measured by MLS was 26.3 ppmv at 100 hPa associated with an overshooting convective event in August 2019 that spanned thousands of square kilometers and persisted for several hours (Werner et al., 2020). Two pyroCbs stand out in the MLS H_2O record: the 2017 Pacific Northwest (Pumphrey et al., 2021) and the 2019/2020 Australian New Year's (Schwartz et al., 2020) events. Only the Australian pyroCbs injected enough H_2O to allow an accurate estimate of mass (19±3 Tg).

The 2008 Kasatochi (Schwartz et al., 2013) and the 2015 Calbuco (Sioris et al., 2016) volcanic eruptions were the only others in the MLS record that injected appreciable amounts of H_2O into the stratosphere. Neither deposited H_2O at altitudes higher than 68 hPa ($\sim$18.6 km), and both injections were too small for a reliable H_2O mass estimate.
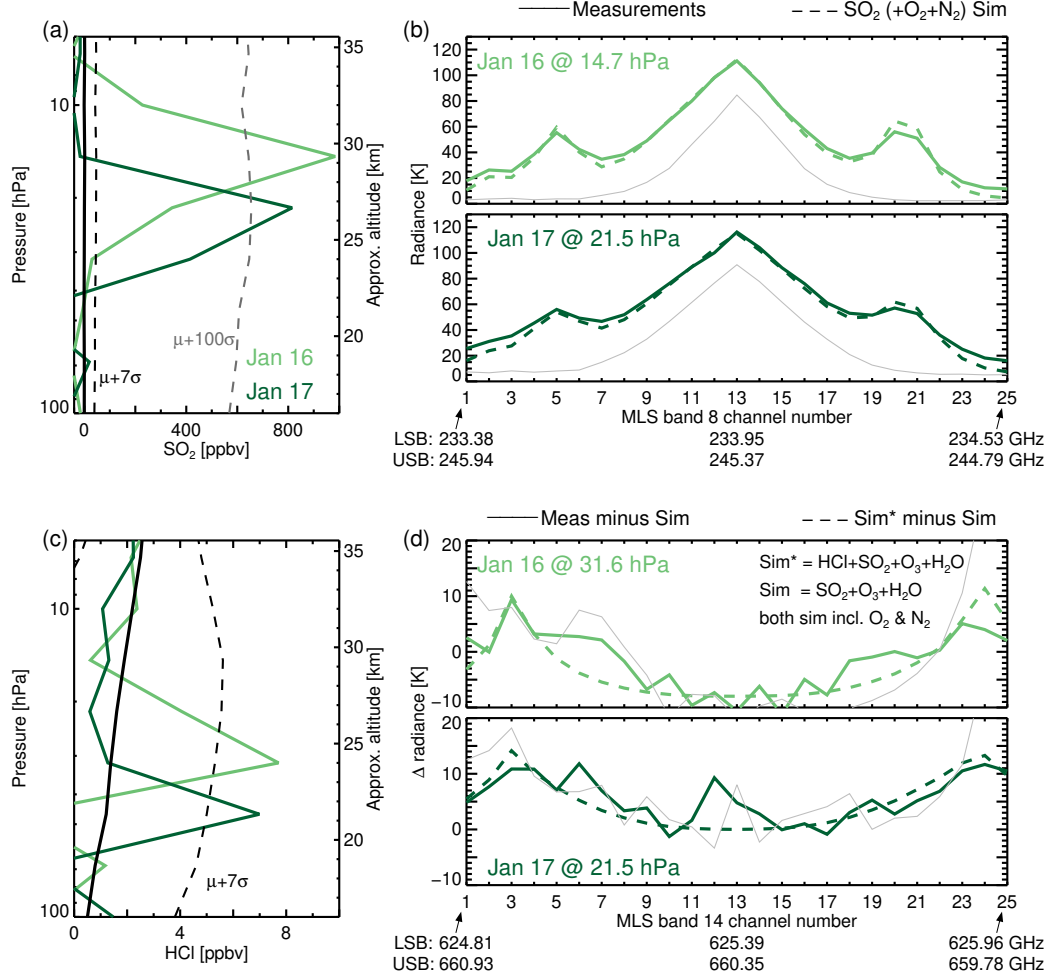
Figure 2. Profiles with maximum (a) SO_2 and (c) HCl on 16 and 17 January. All of these measurements lie downwind of the HT-HH volcano. (b) Measured (solid lines) and simulated (dashed) SO_2 radiances at the mixing ratio maxima for the enhanced profiles (colored lines), as well as for background conditions at the same pressure levels (gray lines). (d) As (b) but for differences between measured radiances and those simulated without HCl (solid lines), as well as estimated HCl signatures (from differences between simulations, see legend; dashed lines). All enhancements shown fail the QS.
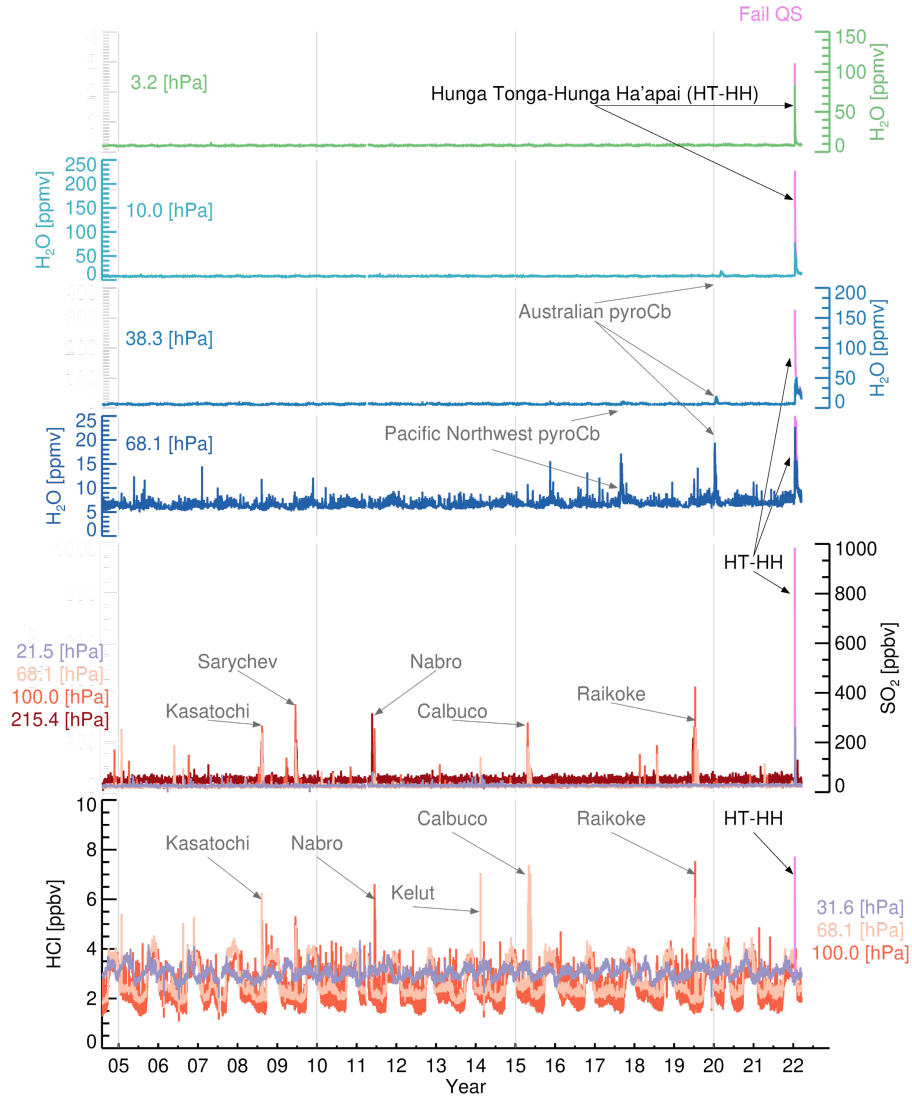
Figure 3. Time series of quality-screened maximum H_2O, SO_2, and HCl mixing ratios at different pressure levels. SO_2 maxima at $14\,hPa$ and HCl maxima at $31\,hPa$ disregarding QS after the HT-HH eruption are shown in pink. Similarly, H_2O maxima disregarding QS are shown in pink for each level.

The HT-HH eruption injected at least 146 ± 5 Tg of H_2O into the stratosphere, not only surpassing the magnitudes of all other injections in the MLS record, but also eclipsing a theoretical estimate of 37.5 Tg from Pinatubo (Pitari & Mancini, 2002). To put the HT-HH injection into perspective, the enhancement represents $\sim$10% of the estimated stratospheric H_2O burden of 1400 Tg (Glaze et al., 1997). Further, the H_2O plume injection height far exceeded that of any other injections in the MLS record (Figure 3).

4 Evolution of the H_2O plume

To study the development of the H_2O plume, Figure 4 shows maps for selected days after the eruption and meridional and zonal mean anomalies based on all data points as well as only those that pass the QS criteria. On 15 January, the plume reached 0.46 hPa ($\sim$53 km), with most of the MLS retrievals failing QS. On 16 January, two separate plumes are visible, one in the upper stratosphere (between 1 and 8 hPa) and the other in the lower stratosphere (between 10 and 80 hPa), where most of the H_2O volume was injected. On this day, the effects on the plume of strong wind shear between 1 and 8 hPa are already apparent.

By 22 January, the plume had almost entirely circled the globe at 2.1 hPa, while only travelling halfway around at 26 hPa. On average, through January and February, the plume moved $\sim$37 degrees longitude per day at 2.1 hPa, but only $\sim$18 degrees longitude per day from 31 to 6 hPa, consistent with winds from meteorological analyses (see Figure S2) interpolated to the MLS measurement times and locations as described by Manney et al. (2007). By 5 February, the plume covered all longitudes, with the largest enhancements from 38 to 21 hPa ($\sim$22 to 26 km). By 31 March, the plume around 4.6 hPa had dropped to near background values.

Measurements from 31 March show the persistence of the H_2O plume in the lower and middle stratosphere. Concurrent with encircling the globe, the H_2O plume broadened slowly, spreading mostly northward around 26 hPa. This plume will require further monitoring as the eruption signal propagates into the upper stratosphere and toward the poles in the Brewer-Dobson Circulation (BDC).

5 Discussion and Summary

The importance of stratospheric H_2O is well established; it affects stratospheric chemistry and dynamics, as well as atmospheric radiation. For example, excess stratospheric H_2O could lead to enhanced OH concentrations, slightly enhancing O_3 production through the CH_4 oxidation cycle but worsening O_3 depletion through the HO_x cycle, leading to a net decrease in O_3 (e.g., Dvortsov & Solomon, 2001; Stenke & Grewe, 2005). The enhanced OH concentrations could also increase the loss of CH_4, resulting in a decrease in its lifetime (e.g., Ko et al., 2013; Stevenson et al., 2020) and thus reducing its long-term effect on climate. In addition, if enhanced H_2O concentrations were to be entrained into the developing Antarctic vortex to an extent sufficient to raise the formation temperature of polar stratospheric clouds, then the earlier onset of heterogeneous processing would exacerbate cumulative chemical O_3 loss. In terms of transport, a study of the dynamical response to a uniform doubling of stratospheric H_2O concluded that such moistening could reduce stratospheric temperature and increase the strength of the BDC; it could also result in the tropospheric westerly jets becoming stronger and storm tracks shifting poleward (Maycock et al., 2013). Since the HT-HH injection is $\sim$10% of the stratospheric H_2O burden, a dynamical response of lesser magnitude than that found by Maycock et al. (2013) would be expected.

H_2O enters the stratosphere primarily in the tropics, where it freeze-dries at the cold point tropopause (Brewer, 1949). This mechanism gives rise to the "tape recorder", whereby the annual cycle in tropopause temperatures is imprinted in alternating bands
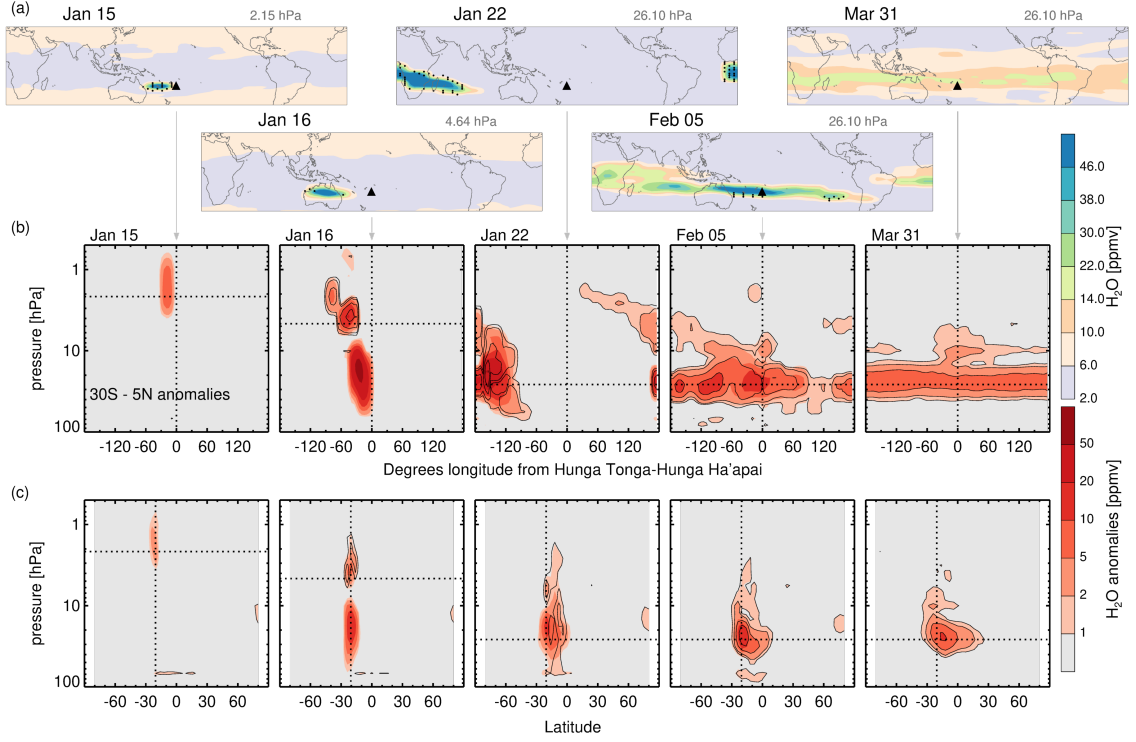
Figure 4. (a) Maps of H_2O at selected pressure levels for illustrative days after the eruption. Stippling indicates regions where a majority of the retrievals do not pass the QS. The volcano location is indicated by a triangle. (b) Meridional (30°S to 5°N) and (c) zonal mean anomalies for the same days. Colored contours show anomalies using all MLS H_2O retrievals, while line contours display the same anomalies based only on QS data; differences indicate regions where many measurements do not pass QS. The volcano location is shown by dashed vertical lines; dashed horizontal lines indicate the level of the map on each day.

of dry and moist air rising in the tropical stratosphere (Mote et al., 1996). By short-circuiting the pathway through the cold point, HT-HH has disrupted this "heartbeat" signal (Figure 5a).

Consistent with the freeze-drying mechanism, unusually low tropopause temperatures around 2001 led to a sharp drop in the amount of H_2O entering the stratosphere (e.g., Randel et al., 2006; Rosenlof & Reid, 2008, Figure 5). This dry anomaly propagated via the BDC (Randel et al., 2006; Urban et al., 2014), slowly rising through the stratosphere and moving towards the poles. Using the propagation of the 2001 H_2O drop as described by Brinkop et al. (2016) as an analogue for the transport of the HT-HH plume, we expect that ascent could carry volcanic H_2O to 10 hPa within ~9 months. The excess H_2O could arrive in northern and southern midlatitudes in ~18 and ~24 months, respectively, over a broad domain in the upper stratosphere. Since part of the plume has entered the lower branch of the BDC, the elevated H_2O may reach lower stratospheric midlatitudes within a few months. The timescale for complete dissipation of the plume may be 5 to 10 years (Hall & Waugh, 1997).

The sudden drop in H_2O of ~0.4 ppmv in 2001 (Figure 5b) demonstrated that the radiative forcing from even small variations in lower stratospheric H_2O can induce changes in global-mean surface temperature (e.g., Solomon et al., 2010). The unprecedented HT-HH enhancement would correspond to ~1.5 ppmv if averaged over 60°S–60°N.

Previous studies of the radiative effects of stratospheric H_2O perturbations, including direct volcanic injection, have shown that they can cause surface warming (e.g., Rind & Lonergan, 1995; Joshi & Jones, 2009). As established in Section 3, the HT-HH eruption was unusual in that it injected extremely large amounts of H_2O. Preliminary model simulations (Figure S3b) suggest an effective radiative forcing (e.g., Forster et al., 2001; Myhre et al., 2013; Wang et al., 2017; Smith et al., 2020) at the tropopause of $+0.15\,\mathrm{Wm^{-2}}$ due to the stratospheric H_2O enhancement. For comparison, the radiative forcing increase due to the CO_2 growth from 1996 to 2005 was about $+0.26\,\mathrm{Wm^{-2}}$ (Solomon et al., 2010).

The HT-HH H_2O enhancement will exert a positive radiative forcing on the surface, offsetting the surface cooling caused by the aerosol radiative forcing (e.g., Zhang et al., 2022; Sellitto et al., 2022). Given the extraordinary magnitude of the HT-HH H_2O injection and the fact that its anticipated stratospheric residence time exceeds the typical 2–3 year timescale for sulfate aerosols to fall out of the stratosphere (Joshi & Jones, 2009), HT-HH may be the first volcanic eruption observed to impact climate not through surface cooling caused by volcanic sulfate aerosols, but rather through surface warming caused by excess H_2O radiative forcing.

In summary, MLS measurements indicate that an exceptional amount of H_2O was injected directly into the stratosphere by the HT-HH eruption. We estimate that the magnitude of the injection constituted at least 10% of the total stratospheric H_2O burden. On the day of the eruption, the H_2O plume reached ~53 km altitude. The H_2O injection bypassed the cold point tropopause, disrupted the H_2O tape recorder signal, set a new record for H_2O injection height in the 17-year MLS record, and could alter stratospheric chemistry and dynamics as the long-lived H_2O plume propagates through the stratosphere in the BDC. Unlike previous strong eruptions in the satellite era, HT-HH could impact climate not through surface cooling due to sulfate aerosols, but rather through surface warming due to the excess stratospheric H_2O forcing. Given the potential high-impact consequences of the HT-HH H_2O injection, it is critical to continue monitoring volcanic gases from this (and future) eruptions to better quantify their varying roles in climate.
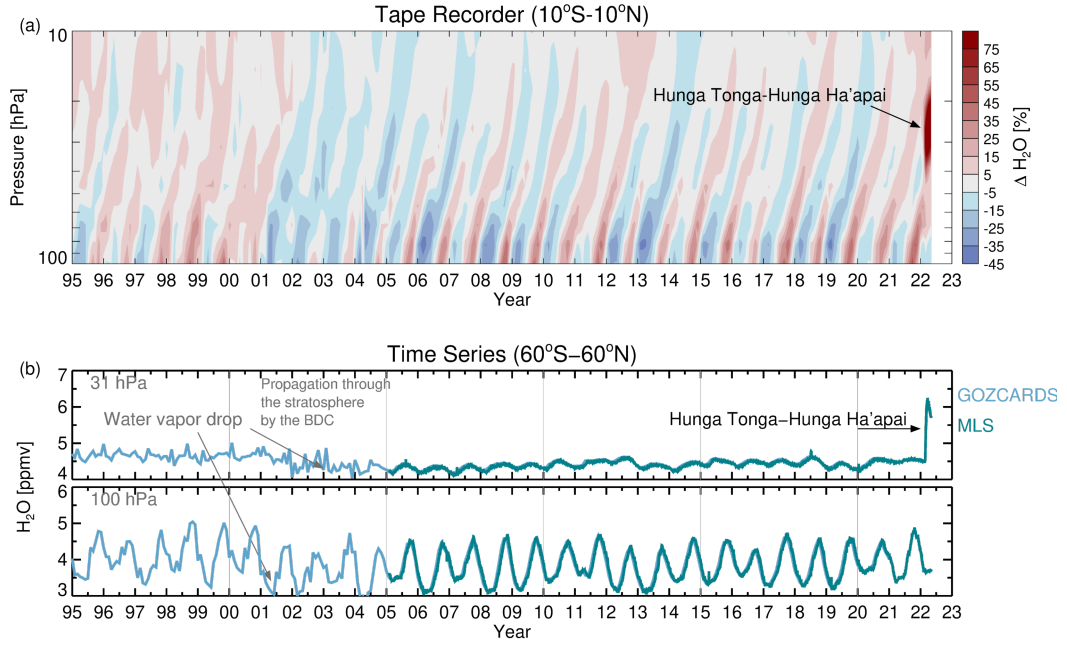
Figure 5. (a) The atmospheric tape recorder (zonal mean H_2O anomalies in the tropics). (b) Time series of near-global (60°S to 60°N) H_2O at 100 and 31 hPa. H_2O abundances are based on GOZCARDS (Froidevaux et al., 2015) and MLS data.

Data Availability Statement

The data sets used here are publicly available, as follows. Aura MLS Level 2 data: `https://disc.gsfc.nasa.gov/datasets?page=1&keywords=AURA%20MLS`; Aura MLS Derived Meteorological Products (DMPs): `https://mls.jpl.nasa.gov/eos-aura-mls/dmp` (registration required).

References

Brewer, A. W. (1949). Evidence for a world circulation provided by the measurements of helium and water vapour distribution in the stratosphere. *Quarterly Journal of the Royal Meteorological Society*, *75*(326), 351–363. Retrieved from `https://doi.org/10.1002/qj.49707532603` doi: 10.1002/qj.49707532603

Brinkop, S., Dameris, M., Jöckel, P., Garny, H., Lossow, S., & Stiller, G. (2016). The millennium water vapour drop in chemistry–climate model simulations. *Atmospheric Chemistry and Physics*, *16*(13), 8125–8140. Retrieved from `https://doi.org/10.5194/acp-16-8125-2016` doi: 10.5194/acp-16-8125-2016

Carn, S., Clarisse, L., & Prata, A. (2016). Multi-decadal satellite measurements of global volcanic degassing. *Journal of Volcanology and Geothermal Research*, *311*, 99–134. Retrieved from `https://doi.org/10.1016/j.jvolgeores.2016.01.002` doi: 10.1016/j.jvolgeores.2016.01.002

Carr, J. L., Horvath, A., Wu, D. L., & Friberg, M. D. (2022). Stereo plume height and motion retrievals for the record-setting Hunga Tonga-Hunga Ha'apai eruption of 15 January 2022. *Geophysical Research Letters*. Retrieved from `https://doi.org/10.1002/essoar.10510365.1` (submitted) doi: 10.1002/essoar.10510365.1

Carvajal, M., Sepúlveda, I., Gubler, A., & Garreaud, R. (2022). Worldwide signature of the 2022 Tonga volcanic tsunami. *Geophysical Research Letters*, *49*(6). Retrieved from `https://doi.org/10.1029/2022gl098153` doi: 10.1029/2022gl098153

Coffey, M. T. (1996). Observations of the impact of volcanic activity on stratospheric chemistry. *Journal of Geophysical Research: Atmospheres*, *101*(D3), 6767–6780. Retrieved from `https://doi.org/10.1029/95jd03763` doi: 10.1029/95jd03763

Cronin, S., Brenna, M., Smith, I., Barker, S., Tost, M., Ford, M., ... Vaiomounga, R. (2017). New volcanic island unveils explosive past. *Eos*. Retrieved from `https://doi.org/10.1029/2017eo076589` doi: 10.1029/2017eo076589

de Leeuw, J., Schmidt, A., Witham, C. S., Theys, N., Taylor, I. A., Grainger, R. G., ... Kristiansen, N. I. (2021). The 2019 Raikoke volcanic eruption – Part 1: Dispersion model simulations and satellite retrievals of volcanic sulfur dioxide. *Atmospheric Chemistry and Physics*, *21*(14), 10851–10879. Retrieved from `https://acp.copernicus.org/articles/21/10851/2021/` doi: 10.5194/acp-21-10851-2021

Dvortsov, V. L., & Solomon, S. (2001). Response of the stratospheric temperatures and ozone to past and future increases in stratospheric humidity. *Journal of Geophysical Research: Atmospheres*, *106*(D7), 7505–7514. Retrieved from `https://doi.org/10.1029/2000jd900637` doi: 10.1029/2000jd900637

Forster, P. M., Ponater, M., & Zhong, W.-Y. (2001). Testing broadband radiation schemes for their ability to calculate the radiative forcing and temperature

response to stratospheric water vapour and ozone changes. *Meteorologische Zeitschrift*, *10*(5), 387–393. Retrieved from https://doi.org/10.1127/0941-2948/2001/0010-0387 doi: 10.1127/0941-2948/2001/0010-0387

Froidevaux, L., Anderson, J., Wang, H.-J., Fuller, R. A., Schwartz, M. J., Santee, M. L., . . . McCormick, M. P. (2015). Global OZone chemistry and related trace gas data records for the stratosphere (GOZCARDS): methodology and sample results with a focus on HCl, H_2O, and O_3. *Atmospheric Chemistry and Physics*, *15*(18), 10471–10507. Retrieved from https://doi.org/10.5194/acp-15-10471-2015 doi: 10.5194/acp-15-10471-2015

Glaze, L. S., Baloga, S. M., & Wilson, L. (1997). Transport of atmospheric water vapor by volcanic eruption columns. *Journal of Geophysical Research: Atmospheres*, *102*(D5), 6099–6108. Retrieved from https://doi.org/10.1029/96jd03125 doi: 10.1029/96jd03125

Hall, T. M., & Waugh, D. (1997). Tracer transport in the tropical stratosphere due to vertical diffusion and horizontal mixing. *Geophysical Research Letters*, *24*(11), 1383–1386. Retrieved from https://doi.org/10.1029/97gl01289 doi: 10.1029/97gl01289

Joshi, M. M., & Jones, G. S. (2009). The climatic effects of the direct injection of water vapour into the stratosphere by large volcanic eruptions. *Atmospheric Chemistry and Physics*, *9*(16), 6109–6118. Retrieved from https://doi.org/10.5194/acp-9-6109-2009 doi: 10.5194/acp-9-6109-2009

Ko, M. K. W., Newman, P. A., Reimann, S., & Strahan, S. E. (Eds.). (2013). *SPARC Report on Lifetimes of Stratospheric Ozone-Depleting Substances, Their Replacements, and Related Species* (Vol. No. 6; Tech. Rep.). SPARC. Retrieved from http://www.sparc-climate.org/publications/sparc-reports/

Kusky, T. M. (2022). Déjà vu: Might future eruptions of Hunga Tonga-Hunga Ha'apai volcano be a repeat of the devastating eruption of Santorini, Greece (1650 BC)? *Journal of Earth Science*, *33*(2), 229–235. Retrieved from https://doi.org/10.1007/s12583-022-1624-2 doi: 10.1007/s12583-022-1624-2

Livesey, N. J., Read, W., Wagner, L., P. A. Froidevaux, Lambert, A., Manney, G. L., Millán Valle, L., . . . R., L. R. (2020). *Version 4.2x Level 2 and 3 data quality and description document* (Tech. Rep. No. JPL D-33509 Rev. E). Jet Propulsion Laboratory. Retrieved from http://mls.jpl.nasa.gov

Livesey, N. J., Santee, M. L., & Manney, G. L. (2015). A Match-based approach to the estimation of polar stratospheric ozone loss using Aura Microwave Limb Sounder observations. *Atmospheric Chemistry and Physics*, *15*(17), 9945–9963. Retrieved from https://acp.copernicus.org/articles/15/9945/2015/ doi: 10.5194/acp-15-9945-2015

Livesey, N. J., Snyder, W. V., Read, W. G., & Wagner, P. A. (2006). Retrieval algorithms for the EOS Microwave Limb Sounder (MLS). *IEEE Transactions on Geoscience and Remote Sensing*, *44*(5), 1144–1155. Retrieved from https://doi.org/10.1109/tgrs.2006.872327 doi: 10.1109/tgrs.2006.872327

Manney, G. L., Daffer, W. H., Zawodny, J. M., Bernath, P. F., Hoppel, K. W., Walker, K. A., . . . Waters, J. W. (2007). Solar occultation satellite data and derived meteorological products: Sampling issues and comparisons with Aura Microwave Limb Sounder. *Journal of Geophysical Research*, *112*(D24). Retrieved from https://doi.org/10.1029/2007jd008709 doi: 10.1029/2007jd008709

Maycock, A. C., Joshi, M. M., Shine, K. P., & Scaife, A. A. (2013). The circulation response to idealized changes in stratospheric water vapor. *Journal of Climate*, *26*(2), 545–561. Retrieved from https://doi.org/10.1175/jcli-d-12-00155.1 doi: 10.1175/jcli-d-12-00155.1

McCormick, M. P., Thomason, L. W., & Trepte, C. R. (1995). Atmospheric effects

of the Mt Pinatubo eruption. *Nature*, *373*(6513), 399–404. Retrieved from `https://doi.org/10.1038/373399a0` doi: 10.1038/373399a0

Mote, P. W., Rosenlof, K. H., McIntyre, M. E., Carr, E. S., Gille, J. C., Holton, J. R., . . . Waters, J. W. (1996). An atmospheric tape recorder: The imprint of tropical tropopause temperatures on stratospheric water vapor. *Journal of Geophysical Research: Atmospheres*, *101*(D2), 3989–4006. Retrieved from `https://doi.org/10.1029/95jd03422` doi: 10.1029/95jd03422

Myhre, G., Shindell, D., Bréon, F.-M., Collins, W., Fuglestvedt, J., Huang, J., . . . Zhang, H. (2013). Anthropogenic and natural radiative forcing. In T. F. Stocker et al. (Eds.), *Climate Change 2013: The Physical Science Basis. Contribution of Working Group I to the Fifth Assessment Report of the Intergovernmental Panel on Climate Change* (pp. 659–740). Cambridge, UK: Cambridge University Press. doi: 10.1017/CBO9781107415324.018

Pinto, J. P., Turco, R. P., & Toon, O. B. (1989). Self-limiting physical and chemical effects in volcanic eruption clouds. *Journal of Geophysical Research*, *94*(D8), 11165. Retrieved from `https://doi.org/10.1029/jd094id08p11165` doi: 10.1029/jd094id08p11165

Pitari, G., & Mancini, E. (2002). Short-term climatic impact of the 1991 volcanic eruption of Mt. Pinatubo and effects on atmospheric tracers. *Natural Hazards and Earth System Sciences*, *2*(1/2), 91–108. Retrieved from `https://doi.org/10.5194/nhess-2-91-2002` doi: 10.5194/nhess-2-91-2002

Proud, S. R., Prata, A., & Schmauss, S. (2022). The January 2022 eruption of Hunga Tonga-Hunga Ha'apai volcano reached the mesosphere. *Earth and Space Science Open Archive*, 11. Retrieved from `https://doi.org/10.1002/essoar.10511092.1` doi: 10.1002/essoar.10511092.1

Pumphrey, H. C., Read, W. G., Livesey, N. J., & Yang, K. (2015). Observations of volcanic SO_2 from MLS on Aura. *Atmospheric Measurement Techniques*, *8*(1), 195–209. Retrieved from `https://doi.org/10.5194/amt-8-195-2015` doi: 10.5194/amt-8-195-2015

Pumphrey, H. C., Schwartz, M. J., Santee, M. L., III, G. P. K., Fromm, M. D., & Livesey, N. J. (2021). Microwave Limb Sounder (MLS) observations of biomass burning products in the stratosphere from Canadian forest fires in August 2017. *Atmospheric Chemistry and Physics*, *21*(22), 16645–16659. Retrieved from `https://doi.org/10.5194/acp-21-16645-2021` doi: 10.5194/acp-21-16645-2021

Ramirez-Herrera, M. T., Coca, O., & Vargas-Espinosa, V. (2022). Tsunami effects on the Coast of Mexico by the Hunga Tonga-Hunga Ha'apai volcano eruption. *submitted*. Retrieved from `https://doi.org/10.31223/x5x33z` doi: 10.31223/x5x33z

Randel, W. J., Wu, F., Vömel, H., Nedoluha, G. E., & Forster, P. (2006). Decreases in stratospheric water vapor after 2001: Links to changes in the tropical tropopause and the Brewer-Dobson circulation. *Journal of Geophysical Research*, *111*(D12). Retrieved from `https://doi.org/10.1029/2005jd006744` doi: 10.1029/2005jd006744

Read, W. G., Froidevaux, L., & Waters, J. W. (1993). Microwave Limb Sounder measurement of stratospheric SO_2 from the Mt. Pinatubo Volcano. *Geophysical Research Letters*, *20*(12), 1299–1302. Retrieved from `https://doi.org/10.1029/93gl00831` doi: 10.1029/93gl00831

Rind, D., & Lonergan, P. (1995). Modeled impacts of stratospheric ozone and water vapor perturbations with implications for high-speed civil transport aircraft. *Journal of Geophysical Research*, *100*(D4), 7381–7396. Retrieved from `https://doi.org/10.1029/95jd00196` doi: 10.1029/95jd00196

Rosenlof, K. H., & Reid, G. C. (2008). Trends in the temperature and water vapor content of the tropical lower stratosphere: Sea surface connection. *Journal of Geophysical Research*, *113*(D6). Retrieved from `https://doi.org/10.1029/`

2007jd009109 doi: 10.1029/2007jd009109

Santee, M. L., Lambert, A., Manney, G. L., Livesey, N. J., Froidevaux, L., Neu, J. L., ... Ward, B. M. (2022). Prolonged and Pervasive Perturbations in the Composition of the Southern Hemisphere Midlatitude Lower Stratosphere From the Australian New Year's Fires. *Geophysical Research Letters*, *49*(4), e2021GL096270. Retrieved from `https://agupubs.onlinelibrary.wiley.com/doi/abs/10.1029/2021GL096270` (e2021GL096270 2021GL096270) doi: https://doi.org/10.1029/2021GL096270

Schwartz, M. J., Read, W. G., Santee, M. L., Livesey, N. J., Froidevaux, L., Lambert, A., & Manney, G. L. (2013). Convectively injected water vapor in the North American summer lowermost stratosphere. *Geophysical Research Letters*, *40*(10), 2316–2321. Retrieved from `https://doi.org/10.1002/grl.50421` doi: 10.1002/grl.50421

Schwartz, M. J., Santee, M. L., Pumphrey, H. C., Manney, G. L., Lambert, A., Livesey, N. J., ... Werner, F. (2020). Australian New Year's pyroCb impact on stratospheric composition. *Geophysical Research Letters*, *47*(24). Retrieved from `https://doi.org/10.1029/2020gl090831` doi: 10.1029/2020gl090831

Sellitto, P., Podglajen, A., Belhadji, R., Boichu, M., Carboni, E., Cuesta, J., ... Legras, B. (2022, April). The unexpected radiative impact of the Hunga Tonga eruption of January 15th, 2022. *submitted*. Retrieved from `https://doi.org/10.21203/rs.3.rs-1562573/v1` doi: 10.21203/rs.3.rs-1562573/v1

Sioris, C. E., Malo, A., McLinden, C. A., & D'Amours, R. (2016). Direct injection of water vapor into the stratosphere by volcanic eruptions. *Geophysical Research Letters*, *43*(14), 7694–7700. Retrieved from `https://doi.org/10.1002/2016gl069918` doi: 10.1002/2016gl069918

Smith, C. J., Kramer, R. J., Myhre, G., Alterskjær, K., Collins, W., Sima, A., ... Forster, P. M. (2020). Effective radiative forcing and adjustments in CMIP6 models. *Atmospheric Chemistry and Physics*, *20*(16), 9591–9618. Retrieved from `https://doi.org/10.5194/acp-20-9591-2020` doi: 10.5194/acp-20-9591-2020

Solomon, S., Rosenlof, K. H., Portmann, R. W., Daniel, J. S., Davis, S. M., Sanford, T. J., & Plattner, G.-K. (2010). Contributions of stratospheric water vapor to decadal changes in the rate of global warming. *Science*, *327*(5970), 1219–1223. Retrieved from `https://doi.org/10.1126/science.1182488` doi: 10.1126/science.1182488

Stenke, A., & Grewe, V. (2005). Simulation of stratospheric water vapor trends: impact on stratospheric ozone chemistry. *Atmospheric Chemistry and Physics*, *5*(5), 1257–1272. Retrieved from `https://doi.org/10.5194/acp-5-1257-2005` doi: 10.5194/acp-5-1257-2005

Stevenson, D. S., Zhao, A., Naik, V., O'Connor, F. M., Tilmes, S., Zeng, G., ... Emmons, L. (2020). Trends in global tropospheric hydroxyl radical and methane lifetime since 1850 from AerChemMIP. *Atmospheric Chemistry and Physics*, *20*(21), 12905–12920. Retrieved from `https://doi.org/10.5194/acp-20-12905-2020` doi: 10.5194/acp-20-12905-2020

Themens, D. R., Watson, C., Žagar, N., Vasylkevych, S., Elvidge, S., McCaffrey, A., ... Jayachandran, P. T. (2022). Global propagation of ionospheric disturbances associated with the 2022 Tonga volcanic eruption. *Geophysical Research Letters*, *49*(7). Retrieved from `https://doi.org/10.1029/2022gl098158` doi: 10.1029/2022gl098158

Urban, J., Lossow, S., Stiller, G., & Read, W. (2014). Another drop in water vapor. *Eos, Transactions American Geophysical Union*, *95*(27), 245–246. Retrieved from `https://doi.org/10.1002/2014eo270001` doi: 10.1002/2014eo270001

Wang, Y., Su, H., Jiang, J. H., Livesey, N. J., Santee, M. L., Froidevaux, L., ... Anderson, J. (2017). The linkage between stratospheric water vapor and surface temperature in an observation-constrained coupled general circulation model.

Climate Dynamics, *48*(7-8), 2671–2683. Retrieved from `https://doi.org/10.1007/s00382-016-3231-3` doi: 10.1007/s00382-016-3231-3

Waters, J., Froidevaux, L., Harwood, R., Jarnot, R., Pickett, H., Read, W., . . . Walch, M. (2006). The Earth Observing System Microwave Limb Sounder (EOS MLS) on the Aura satellite. *IEEE Transactions on Geoscience and Remote Sensing*, *44*(5), 1075–1092. Retrieved from `https://doi.org/10.1109/tgrs.2006.873771` doi: 10.1109/tgrs.2006.873771

Werner, F., Schwartz, M. J., Livesey, N. J., Read, W. G., & Santee, M. L. (2020). Extreme outliers in lower stratospheric water vapor over North America observed by MLS: Relation to overshooting convection diagnosed from colocated Aqua-MODIS data. *Geophysical Research Letters*, *47*(24). Retrieved from `https://doi.org/10.1029/2020gl090131` doi: 10.1029/2020gl090131

Wright, C., Hindley, N., Alexander, M. J., Barlow, M., Hoffmann, L., Mitchell, C., . . . Yue, J. (2022). Tonga eruption triggered waves propagating globally from surface to edge of space. *Earth and Space Science Open Archive*, 23. Retrieved from `https://doi.org/10.1002/essoar.10510674.1` doi: 10.1002/essoar.10510674.1

Yuen, D. A., Scruggs, M. A., Spera, F. J., Zheng, Y., Hu, H., McNutt, S. R., . . . Tanioka, Y. (2022). Under the surface: Pressure-induced planetary-scale waves, volcanic lightning, and gaseous clouds caused by the submarine eruption of Hunga Tonga-Hunga Ha'apai volcano. *Earthquake Research Advances*, 100134. Retrieved from `https://doi.org/10.1016/j.eqrea.2022.100134` doi: 10.1016/j.eqrea.2022.100134

Zhang, H., Wang, F., Li, J., Duan, Y., Zhu, C., & He, J. (2022). Potential impact of Tonga volcano eruption on global mean surface air temperature. *Journal of Meteorological Research*, *36*(1), 1–5. Retrieved from `https://doi.org/10.1007/s13351-022-2013-6` doi: 10.1007/s13351-022-2013-6